CIRCULAR POLARIZATION IN A SOLAR FILAMENT

JINGXIU WANG[1], GUIPING ZHOU[1,2], YUMING WANG[1,3] and LIMIN SONG[1,4]
[1]*National Astronomical Observatories, Chinese Academy of Sciences, Beijing 100012, China*
[2]*Anhui University, Hefei 230039, China*
[3]*University of Science and Technology, Hefei 230026, China*
[4]*Beijing Normal University, Beijing 100875, China*

(Received in final form 28 April 2003)

Abstract. Integrating 26 624 pairs of video frames, the authors have mapped the circular polarization in an active-region filament against the solar disk by using a traditional magnetograph working at the Hβ line. This filament, offset the disk center, appeared at the boundary of three decayed active regions. It was quiet and away from any strong enhanced network. The mapped circular polarization in the filament has an average polarization degree of 1.1×10^{-3} with a measurement precision of 4×10^{-4}. The mapping of circular polarization in a filament may provide a supplementary diagnosis of the filament magnetic field, in addition to the mapping of linear polarization via the Hanle effect. However, the interpretation of the circular polarization requires treatment of the full quantum problem of Zeeman and non-Zeeman effects of Stokes line profiles.

1. Introduction

One of the most important physical parameters in solar filaments (seen against the solar disk) or prominences (seen above the solar limb) is the magnetic field which permeates all the filamentary threads. The field strength, topology and temporal evolution are intrinsically related to the morphology, dynamics, and activity of filaments. This recognition goes back to Hale (1913) when the strong magnetic field in sunspots had just been diagnosed for 5 years. Before the actual measurements of magnetic fields in prominences, Kippenhahn and Schlüter (1957) already proposed a model of magnetic configuration in which the prominence plasma sits in the dip of the magnetic lines of force connecting to the opposite polarity fields on both sides of the magnetic neutral line. In this K–S model, the magnetic field underneath the prominence follows the direction from the positive to negative polarity in the photosphere. Thus, it is referred to as *normal polarity* configuration. Later, Kuperus and Raadu (1974) suggested an alternative model, in which the plasma was supported by the closed magnetic lines of force. This K–R model predicts that the magnetic field beneath the prominence goes from the negative to positive polarity, referring to the photospheric neutral line. Accordingly, it is referred to as *inverse polarity* configuration.

The first measurements of magnetic fields in solar prominences were made by Zirin and Severny (1961) based on the Zeeman effect. They were followed

Solar Physics **216:** 143–157, 2003.

by the extensive measurements of magnetic fields in prominences in the 1960s. Rust (1967) presented the results for about 100 quiescent prominences; Harvey (1969) summarized the measurements for more than 200 active-region prominences. Those pioneer efforts have fairly established that the magnetic field in prominences falls in the range from several to approximately 200 G, and the field in active-region filaments is many times larger than that in quiescent filaments; the direction of magnetic field seems to be, more or less, along the axis of the elongated filaments. Very recently, Brown, López Ariste, and Casini (2003) explored the possible effects of atomic polarization on those early measurements.

Polarization measurements of solar prominences based on the Hanle effect were first made by Leroy, Ratier, and Bommier (1977), and were carried out extensively later by Leroy, Bommier, and their co-workers. Leroy, Bommier, and Sahal-Bréchot (1983, 1984) presented vector magnetic field measurements via the Hanle effect in hundreds of prominences, including polar crown prominences as well as medium and low latitude prominences. They have concluded that the prominences with height larger than 30 000 km have *inverse polarity* and field strength of 5–10 G, while the prominences of lower height have rather stronger field and *normal polarity*. In either case, they have found that the magnetic vector is not far from the horizontal plane and makes a small angle (20–25 deg) with the long axis of the prominences. Note, their *normal (inverse) polarity* is referring to *the most probable field vector*, oriented from positive (negative) photospheric polarity toward negative (positive) polarity, and seems not to be exactly the same as that predicted by the K–S and K–R models.

Although most observations have claimed that there is a dominant field component along the filament long axis and within, more or less, the horizontal plane (Rust, 1967; Harvey, 1969; Tandberg-Hanssen, 1974; Athay *et al.*, 1983; Leroy, Bommier, and Sahal-Bréchot, 1984), inclined magnetic fields in quiescent prominences were reported by Athay *et al.* (1983) and Bommier, Leroy, and Sahal-Bréchot (1986). Lin, Penn, and Kuhn (1998) reported that in one section of a filament the axial component of the magnetic field reversed on either side of the filament axis. Kim *et al.* (1990) suggested that there were two systems of magnetic fields: one oriented opposite to the underlying photospheric field and crossing the filament long axis at a small angle; the other was coincided with the underlying field and perpendicular to the filament axis. The internal magnetic structures in filaments seem to be far more complicated than current understanding.

Since the measurements of magnetic field in filaments needs great improvement, the discussion on the internal magnetic structure and environmental magnetic configuration of filaments is an exciting topic in solar physics. As an example, the magnetic chirality and its global regularities in filaments have drawn great attention (Low, 1996; Zirker *et al.*, 1997; Martin, 1998; Foukal, 1998), but debates exist on many aspects of the intrinsic magnetic structure in filaments. In this aspect, it is not definitively known if the carefully statistical determination of the field direction by Leroy, Bommier, and Sahal-Bréchot (1984) could be taken for granted. On the

other hand, it is not clear how safe one can use the 'chirality law', i.e., dextral filaments for northern solar hemisphere and sinistral for southern hemisphere (see Martin, 1998), to resolve the ambiguity in the field direction in Hanle measurements (Bommier and Leroy, 1998). More extensive and accurate measurements of magnetic fields in filaments are clearly demanded. As addressed by Foukal (1998), more synthetic or composite studies are of particular importance.

The observations of magnetic fields in filaments against the solar disk are of importance in learning the magnetic structure in filaments and the filament magnetic environment. On-disk measurements not only provide a different viewing angle of the magnetic field in filaments as comparing with the measurements in prominences, but also facilitate a detailed comparison with the photospheric magnetic fields surrounding the filament. Lin, Penn, and Kuhn (1998) made the first polarization observations of a filament against the solar disk based on the Hanle effect. Trujillo Bueno *et al.* (2002) revealed the presence of magnetic fields of order of a few gauss that were highly inclined with respect to the solar radius vector in filaments, by using Hanle-based diagnostics. Harvey (2001, private communication) identified a case in which the circular polarization could be clearly seen in a high sensitivity chromospheric magnetogram. Here we present an unambiguous mapping of the circular polarization in an active region filament against the solar disk via a traditional longitudinal magnetograph using the chromospheric Hβ line. The mapping of circular polarization in a filament may provide a potential diagnosis of magnetic fields in filament in addition to Hanle measurements.

2. Observations

The observations were made on 5 October 2001, at Huairou Solar Observing Station of the National Astronomical Observatories in China. A sub-image of a full-Sun Hα filtergram, taken by a 14 cm telescope and a 2k $\times$ 2k CCD at Huairou, is shown in the lower panel of Figure 1, in comparison with the MDI magnetogram taken at the closest time in the upper panel. The filament was rather quiet and located approximately at 400 arc sec S 530 arc sec E. Projected on the solar surface, the filament axis crossed the line of sight at an angle of about 60.0 deg. However, in the vertical extent, the angle between the line of sight and the filament long axis was estimated to be 32.5 deg (see Figure 2).

The magnetic environment of the filament is synthesized from the MDI magnetograms, and is drawn in Figure 3. The filament was formed in the boundaries of 3 decayed bipole regions, which was consistent with an early discovery (Tang, 1987) that the majority of filaments appeared between active regions.

The polarization measurements described in this study were made by the Solar Magnetic Field Telescope (SMFT), a vector magnetograph system. The advantage of this system is being able to work either at the photospheric line, Fe I 5324 Å, for vector field measurements in the photosphere, or at the chromospheric line,

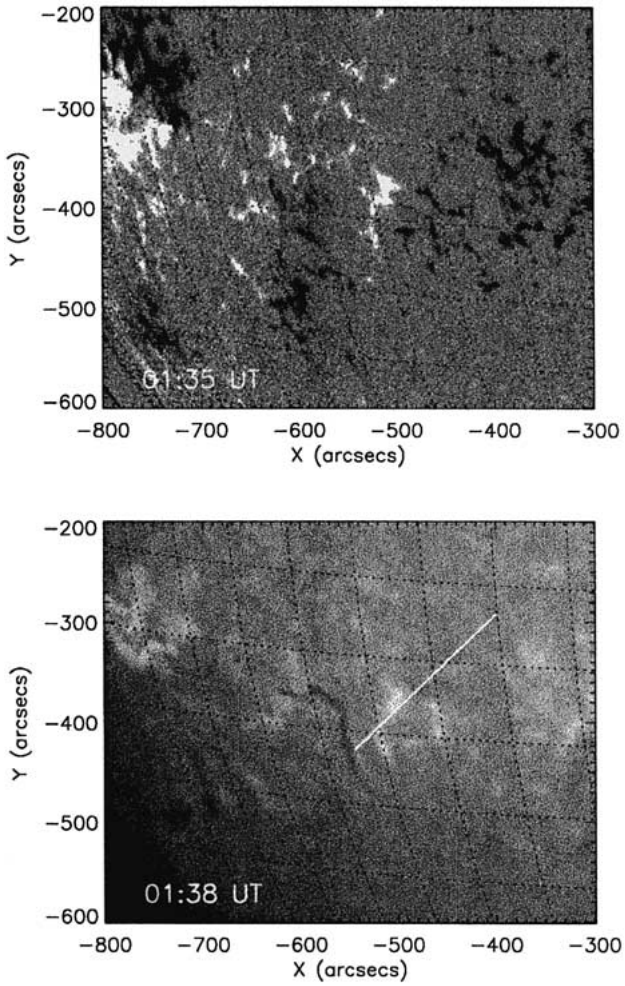

Figure 1. Lower panel: a sub-image of full-Sun Hα filtergram. The *white straight line* represents the line-of-sight direction, and indicates the target filament. *Upper panel*: a segment of a MDI magnetogram of the same scale and at the closest time.

Hβ, for line-of-sight field measurements in the chromosphere (Ai and Hu, 1986; Wang, Ai, and Deng, 1996). Zhang and Ai (1986) have synthesized the Hβ Stokes V profile by solving the Unno–Beckers equations of radiative transfer based on the VAL quiet chromosphere model. The effects of microscopic electric field, Doppler broadening and radiative damping were considered and the perturbation theory of quantum mechanics was used in determining the broadening mechanism and absorption coefficients. The synthetic Stokes I and V profiles were used for Hβ magnetogram calibration in routine observations. Later, two independent examinations of the Hβ magnetogram calibration were made by Liu, Wang, and Yan (1995) and Wang, Ai, and Deng (1996) by using solar rotation observations as well

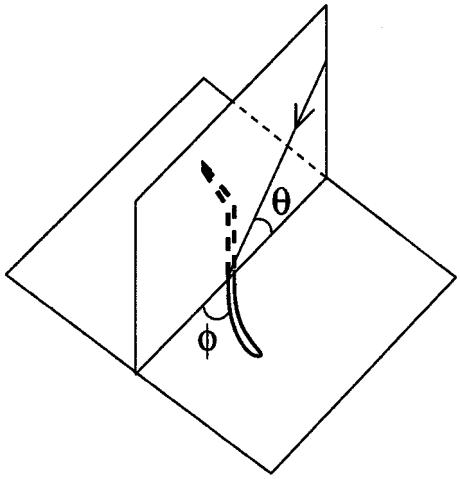

Figure 2. Schematic drawing of the filament alignment. The *horizontal plane* represents the local solar surface. The *long arrow* indicates the line-of-sight direction. Here, $\phi = 60.0°$ and $\theta = 32.5°$.

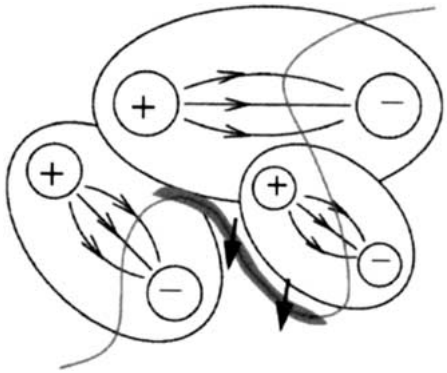

Figure 3. Schematic drawing of the filament environment. The two heavy *arrows* represent the line-of-sight direction. Each bipole region is represented by an oval in which two polarities and the magnetic lines of force are sketched.

as the average observed Hβ line profile. The latter authors suggested an empirical calibration

$$H_{\parallel} = C_H \frac{I_R - I_L}{I_R + I_L} \simeq C \left(\frac{V}{I} \right), \tag{1}$$

where $I_{R,L}$ represented the images of right and left circular polarization, respectively, and C_H was a constant of $(5.2–5.4) \times 10^4$. The empirical and theoretical calibrations differed by a factor of approximate 1.1. In this work the theoretical calibration used in the routine observations at Huairou Solar Observing Station is simply adopted without the indicated correction. Sánchez Almeida (1997) simulated the performance of the Hβ magnetograph by using the exact filter position, -0.24 Å from the line center, and the bandpass from the synthetic Stokes I and V

profiles given by a simple treatment of radiative transfer. He found that unless there was a weak emission core in the Hβ line, the magnetograph performance would be reasonable.

To avoid misleading, it is worth mentioning that in the following observational descriptions we have put the data interpretation aside. *We use the terms of magnetogram and magnetic flux density in usual sense for the active region and plage fields, but in implying only the measure of circular polarization for the filament.*

Although the Hβ line has been successfully used in early measurements of circular polarization in solar prominences based on Zeeman effect (see Harvey, 1969), measurements in filaments become difficult since the photon noise is larger in the later case. Unfortunately, during the observation the seeing at Huairou was not very good.

To greatly enhance the sensitivity of polarization measurements, 26 624 pairs of video frames were integrated to construct the Hβ magnetogram at the expense of temporal resolution. Each pair of I_R and I_L was taken quasi-simultaneously to construct a primitive magnetogram. The interval to get such a primitive magnetogram was 0.16 s. Each 512 primitive magnetograms were automatically integrated to form a deep magnetogram before being written into the hard disk. The total of 52 groups of such deep magnetograms were taken continuously for the filament. Before constructing the final Hβ magnetogram, the 52 magnetograms were co-aligned by cross correlation technique. The noise level of the final magnetogram was estimated from the average signals in the magnetogram in areas in which there were no clear magnetic signals in both photospheric and chromospheric magnetograms. It measured approximately 10 G. About 90 min were used in reconstructing the final magnetogram. Due to the long integration, the fine structures of fast changes in the filament were smeared out. Thus, the magnetogram only presents the smoothed average polarization in the filament. However, the magnetic fields in the filament environment have been mapped with high sensitivity. The spatial resolution of the final Hβ magnetogram was estimated to be less than or close to 5 arc sec.

The resultant Hβ magnetogram for the filament is shown in the upper-right panel of Figure 4 in comparison with the narrow band Hβ filtergram on its left and the corresponding photospheric magnetogram below. A segment of the MDI magnetogram taken at the closest time is presented in the lower-left panel. The two photospheric magnetograms show almost identical magnetic structures. Huairou magnetogram seems to be less noisy, but more diffuse for some stronger magnetic features. The average flux density of the Huairou magnetogram is higher than that of MDI magnetogram by a factor of 1.6.

Comparing the Hβ magnetogram with the two photospheric magnetograms, the expansion of enhanced network from the photosphere to chromosphere, i.e., the canopy effect, is clearly seen. In addition to the expansions of photospheric magnetic structures, the circular polarization in the filament was mapped in the Hβ magnetogram above the neutral zone of the photospheric magnetogram. The polarization appears in the sense of negative in polarity (with field vector away

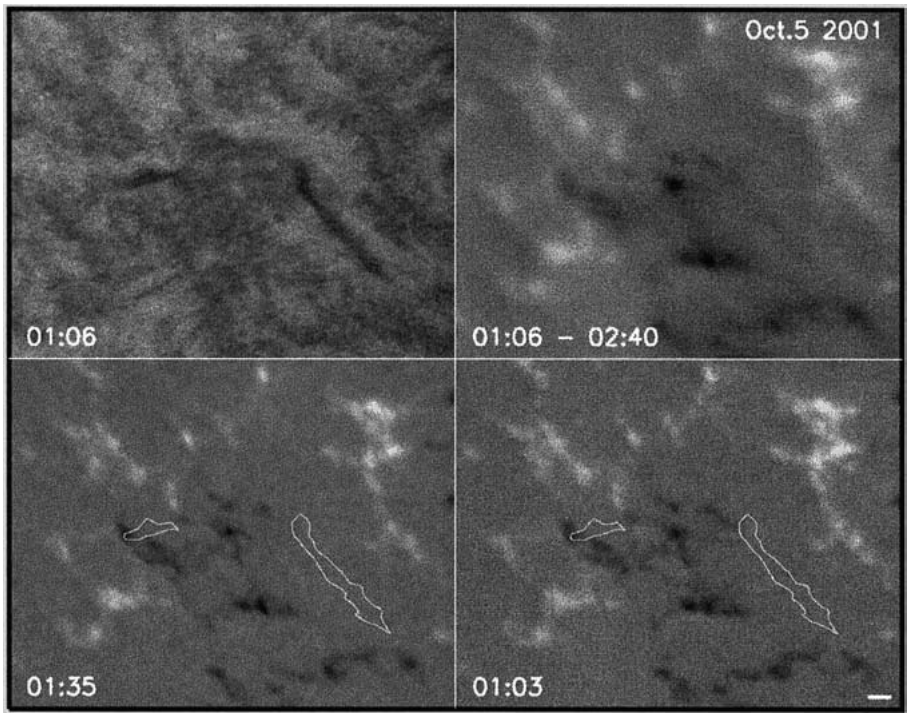

Figure 4. Upper-left panel: off-band Hβ filtergram at -0.24 Å from the line center. *Upper-right panel*: corresponding Hβ magnetogram with integrating 26 624 pairs of video frames. *Lower-left panel*: segment of MDI magnetogram of the same field of view. *Lower-right panel*: corresponding photospheric magnetogram with integration of 512 pairs of video frames. North is at the top, east at the left. A *short bar* at the lower-right corner indicates the scale of 10 arc sec.

from the observer). Measured from the central dark part of the filament, the average polarization signal in the filament was -30.7 G with a standard deviation of 24.3 G. However, measured from the same positions in the magnetic neutral zone in the photosphere, a very low flux density of -0.1 ± 23.4 G was found.

The very deep Hβ magnetogram has unambiguously mapped the circular polarization in the filament at a polarization magnitude of 1.1×10^{-3} above the photospheric neutral zone. The precision of the mapping is 0.4×10^{-3} in polarization magnitude. To show the detailed distribution of the magnetic field, a histogram of the circular polarization in the filament is presented in the upper panel of Figure 5, and the histogram of flux density in the neutral zone of the photosphere in the lower panel. The two histograms present obviously distinct distributions of polarization.

It was noticed that the appearances of the filament in Hα and Hβ filtergrams were not exactly same. In the Hβ filtergram the main body of the filament was clearly shown, but the middle part was fuzzy or missing, while the extreme east part appeared in the form of dark ejecta. However, in the Hα filtergrams, the fila-

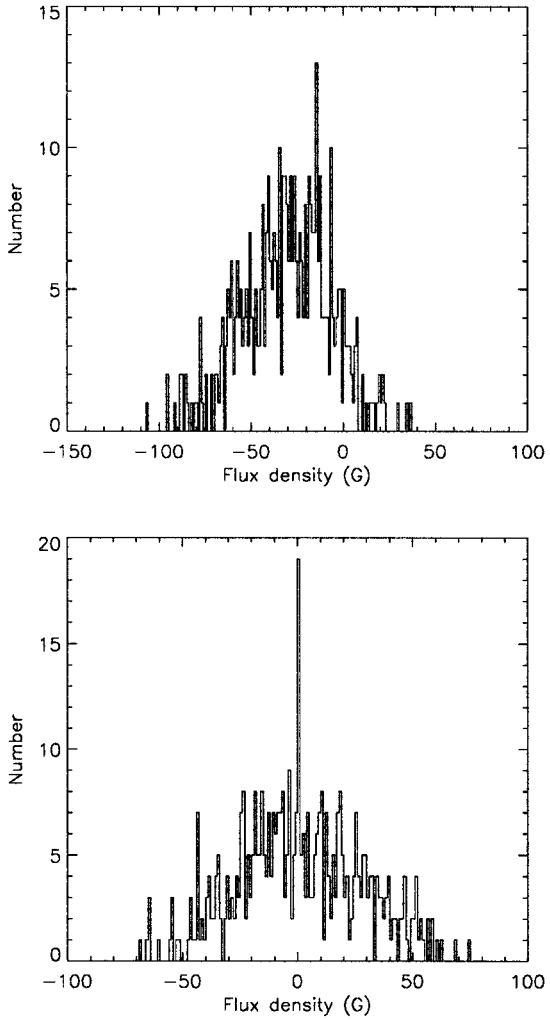

Figure 5. Upper panel: histogram of circular polarization in the central part of the filament. *Lower panel*: histogram of flux density beneath the filament in the photosphere.

ment was observed as rather continuous dark features. Only the main body of the filament presented rather strong polarization.

3. Interpretation of the Data

3.1. Validity of the observation

There are several error sources which may render the observations unreasonable.

First, if the switch from I_R to I_L in the data acquisition was not perfect, then there would be spurious polarization signals in addition to the polarization of the filament. In the SMFT system the modulation from left to right circular polarization is made by KD*Ps which are operated at a constant temperature, 42.24 ± 0.01 °C. They have been working very well since 1987. Their performance at the Hβ line was justified by the comparisons of many thousands of quasi-simultaneous Hβ magnetograms and photospheric magnetograms for various types of solar regions. Zhang and Zhang (2000) demonstrated the general similarities between chromospheric and photospheric magnetograms, even for the weak intra-network magnetic elements. By comparing the chromospheric magnetogram with MDI and Huairou photospheric magnetograms shown in Figure 4, one can identify almost all the counterparts of photospheric magnetic features in the corresponding places of the Hβ magnetogram. This proves that the Hβ magnetograph at Huairou has good performance.

Secondly, if the I_R and I_L were mis-matched in subtraction and addition, there would be fringes of opposite polarities on the outer edges of the filaments. However, this has not been found in the resultant $H\beta$ magnetogram. The I_R and I_L were acquired almost simultaneously. There would be no obviously additional distortion and shift from I_R to I_L during such a short interval. The long integration to construct the final Hβ magnetogram did introduce some smearing of the magnetic features, but the polarization signals should be co-spatial with the filament.

The third question is whether or not there was leakage of linear polarization in the observed Stokes V signals. The Stokes Q and U signals from Zeeman effect are weak, and should not contribute significantly. In the case of scattering polarization, the V signals are much weaker than Q and U signals (Lin, Penn, and Kuhn, 1998; Landi Degl'Innocenti, 1982). For the $H\beta$ line, Bommier, Leroy, and Sahal-Bréchot (1986) found 'an invariably smaller polarization degree, with an average value of 5×10^{-3}'. In the SMFT system, one KD$*$P serves as a quarter-wave plate to prohibit cross-talking between linear and circular polarizations. A careful comparison of Huairou, Big Bear, and Mees vector magnetograms revealed a cross-talking of the SMFT system at the level of 2% (Wang *et al.*, 1992). The leakage of scattering linear polarization will not contribute significantly to the observed circular polarization. The observation presents the first clear case that the circular polarization in a filament has been mapped against the solar disk.

3.2. Polarization mechanism

The polarization mechanism of Hβ in a filament is a complicated, unresolved issue. Both the longitudinal and transverse Zeeman effects and Hanle effect play

roles in the polarized emission. Bommier, Leroy, and Sahal-Bréchot (1986) calculated the linear polarization of the Hβ line by resonant scattering of the anisotropic photospheric and chromospheric radiation field, and de-polarized by the local magnetic field (i.e., the Hanle effect) in prominence. They identified that the Hβ polarization was sensitive to collisions with charged particles, which suggested an unexpected de-polarization mechanism and indicated possibly the importance of the non-scattering Zeeman effects. Moreover, the Hanle effect is only part of the quantum mechanism (QM). The alignment-to-orientation transfer mechanism (Kemp mechanism) has also to be involved in order to interpret the observed circular polarization (Brown, López Ariste, and Casini, 2003). The Kemp effects bring an intensity-like profile in the usual anti-symmetric Stokes V profile from the Zeeman effect, which make the interpretation of circular polarization much more complicated (Landi Degl'Innocenti, 1982). Following Landi Degl'Innocenti, ignoring the influence of Hanle effects, even for the extremely simplified case the Stokes V profile would appear as

$$V = vI(\lambda) + w\frac{\partial I(\lambda)}{\partial \lambda}, \tag{2}$$

where the v depends on the amount of orientation presented in the excited atom, while w depends on the Zeeman splitting. Therefore, the usual interpretation of magnetograph signal does not work when Kemp effects are present. So far, no consistent theoretical treatment of the full quantum problem has been made in the Hβ line formation by taking into account of both Zeeman and other non-Zeeman QM effects.

The relevant contributions of Zeeman and non-Zeeman effects depend intrinsically on the Hβ line formation mechanism. Non-Zeeman effects can occur when coherent scattering or anisotropic radiation 'pumping' processes contribute to the formation of a spectral line (Lin, Penn, and Kuhn, 1998; Trujillo Bueno *et al.*, 2002).

To our knowledge, Heasley and Milkey (1978) presented the first complete theoretical treatment of hydrogen line formation in prominences. They have shown that the radiative cascades and recombination must be included in the statistical equilibrium equations. Those are non-scattering, in fact. These authors noted that the most uncertain aspect in their modeling is the accuracy to which we know the illuminating radiation incident on the prominences. Heinzel, Gouttebroze, and Vial (1987) demonstrated that the nature of the frequency redistribution in the scattering process played an important role in the reconstruction of prominence models. Gouttebroze, Heinzel, and Vial (1993) showed in their extensive calculations that both the frequency redistribution in the scattering process and correct incident radiations were absolutely necessary to obtain a reasonable reproduction of observed profiles. Neither complete frequency redistribution, nor resonant scattering of incident radiation is true in the spectral line formation of prominences.

In an analysis of 10 well-observed solar prominences, Wang and Shi (1983) found that the optical depth of the Hβ line fell in the range of 0.45 to 7.6 with

a mean of 3.6. The coherent scattering could not play a dominant role in the line formation. A diagnosis of the relative importance of scattering and thermal source terms, which was independent of the radiation field, to the line formation (Mihalas, 1978) was also made by Wang and Shi (1983). They demonstrated that the source function changes with optical depth of the emission lines could be approximated as

$$S'_{ji}(\tau) = \frac{\beta_{ji}}{2\sqrt{\pi}} \int_{-\infty}^{\infty} \mathrm{d}x \int_{\tau}^{\tau_{ji}-\tau} [S_{ji}(\tau + W) - J_{ji}^{\odot}\omega_{ji}^{\odot}\gamma_{ji}(x)]\alpha^2 \frac{e^{(-\alpha W)}}{W}\,\mathrm{d}W, \qquad (3)$$

where β_{ji} was the probability of a photon remaining in the same transition, τ_{ji} was the total optical depth for the line transition from i to j, $J_{ji}^{\odot}$ was the intensity of the incident radiation, $\omega_{ji}^{\odot}$ was the dilution factor, $\gamma_{ji}(x)$ the Fraunhofer line profile, and α, the Doppler line profile. Depending on whether or not the local thermal source was dominant, the source function would increase or decrease with optical depth. The authors found that 4 of the 10 prominences showed source function increase with optical depth, 4 showed decrease, another 2 had a constant source function. This indicates that the scattering term and thermal term, in general, play roughly equal roles. Moreover, as the optical depth of Hβ line is not optically thin, the scattering can not be coherent, i.e., intensities at all frequencies are likely to be coupled to some degree.

Although we can not draw a definitive conclusion, Zeeman effects seem to play some important role in the polarization. Therefore, at least a significant fraction of the mapped circular polarization comes from the line-of-sight magnetic fields in the filament. However, without a solid understanding of the polarization mechanism of the filament in the Hβ line, especially a calculation on the relative contribution to the circular polarization signals from Zeeman and non-Zeeman effects, we can not properly answer the question if the mapped circular polarization results predominately from the line-of-sight filament magnetic field via the Zeeman effect.

The deficiency in our current theoretical understanding on the polarization mechanism rules out an accurate interpretation of the circular polarization in the filament. It is likely that Zeeman and Hanle effects may contribute roughly equally to the observed circular polarization. Unfortunately, a quantum theory of filament polarization in Hβ line does not exist. The truly quantitative interpretation of the observed polarization presents a real challenging problem. To combine the Zeeman measurements and the measurements based on the non-Zeeman effects, e.g., Hanle and Kemp effects, may open a door to understand correctly the magnetism and dynamics of filaments.

TABLE I
Magnetic helicity of filament.

Chirality	Polarity distribution	Twisting sense	Magnetic helicity
Dextral	Normal	Right-handed	>0
	Inverse	Left-handed	<0
Sinistral	Normal	Right-handed	<0
	Inverse	Left-handed	>0

4. Discussion on the Magnetic Structure in the Filament and Filament Environment

4.1. A REMARK ON THE INTERNAL STRUCTURE

Unfortunately the polarization measurement in this work only indicated that there was a field component in the filament which was along the line-of-sight and away from the observer. It could not tell if this component was the projection of the horizontal field along the filament long axis, or projection of a vertical field, or projections of both in the filament. Assuming it came from the projection of a predominant field along the long axis, then according to Martin (1998) the filament was sinistral in chirality (see Figure 3), consistent with the chirality law of quiescent filaments in the southern hemisphere. Given the uncertainties in the polarization mechanism, it should be stated that all the discussions based on the measured circular polarization are valid only if future works clarify the relative importance of the two polarization mechanisms.

However, a remark can be made that *the chirality, i.e., dextral and sinistral of filaments, in fact, does not tell the sense of helical structure, or the magnetic helicity in filaments if the supporting field configuration, i.e., K–S or K–R type, is not known*. In Table I, four different types of filaments in the term of magnetic helicity are listed. Given the four possible types of filament, there appears an intriguing question why we can have the global pattern of filaments: the northern filaments are dominantly dextral and with negative helicity, while the southern ones, sinistral and with positive helicity (see Martin, 1998). To account for the global pattern of filaments, the only possibility is that the majority of filaments have an inverse polarity distribution, i.e., K–R configuration. Certainly, the conjecture needs to be further examined. The internal structure in filaments seems still beyond our grasp. Cautions need to be taken when talking about the helical sense or helicity of a filament.

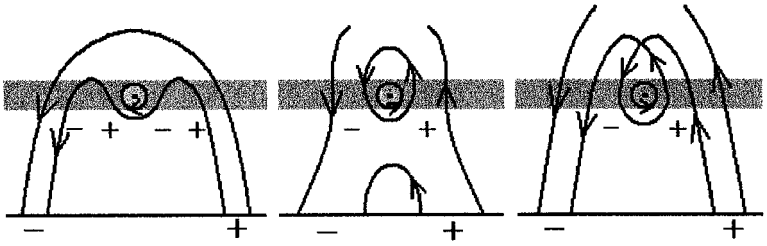

Figure 6. Left: schematic drawing of K–S filament. *Middle and right*: K–R filament. The *small circle* represents the sinistral filament with an axial field pointing to the readers and a helical field rotating in the indicated sense. The *shaded part* represents a layer where the filament forms and the chromospheric magnetic field is mapped. The dark lines of force represent the environment magnetic fields which are connected to the photosphere and support the filament.

4.2. A POSSIBLE DIAGNOSIS OF FILAMENT ENVIRONMENT FIELD

Although the very deep chromospheric magnetogram presented in Figure 4 tells little about the internal field of the filament, it does provide a possibly diagnosis on the filament environment field. As the magnetic field in the layer where the filament formed has been mapped, one can get hints about the configuration of the magnetic fields which support the filament. The helical field in the filament and the fields which were supporting the filament should be in the same direction as they contact each other; otherwise the magnetic reconnection would rapidly destroy the filament. This is why we only list four types of filaments in Table I. The environment magnetic fields supporting the filament, in fact, are in strong field scheme as they are directly connected to the photosphere. They should be detected by the very deep chromospheric magnetogram. If the filament is of K–S type, one might be be able to detect a bipole on either side of the filament in the chromosphere (see the left panel of Figure 6), which, however, would not appear in the photosphere; while for the K–R filament, instead of a bipole some unipolar features might appear additionally on either side of the filament (see the middle and right panels of Figure 6).

Unfortunately, either the predicted bipole or the unipolar features on each side of the filament was not shown in the deep Hβ magnetogram. Although it could not be excluded that the resolution and sensitivity of the Hβ magnetogram were not appropriate to record the predicted supporting fields, the absence of the supporting fields might, on the other hand, indicate more complicated models of filament magnetism, such as that predicted by the flux rope model of Rust and Kumar (1994), or by the model of closely packed flux bundles suggested by Martin and McAllister (1997). A filament seems to support itself by its own internal fields, and not by either magnetic dips or helical fields surrounding the filament.

5. Summary

The circular polarization of an active-region filament has been mapped from an Hβ magnetogram with an integration of 26 624 pairs of video frames. Analysis indicates that a significant fraction of the circular polarization likely originates from the line-of-sight magnetic field in the filament. However, the Kemp effects may prohibit an accurate interpretation of the measurement. However, the work has demonstrated that the circular polarization in the filament at the level of 1×10^{-3} can be unambiguously mapped with the technique based on the traditional magnetograph.

The very deep Hβ magnetogram failed to detect the magnetic fields in the filament neighborhood, which are expected to support the filament in either the K–S or K–R filament models. This may, on the other hand, indicate a more complicated model of filament magnetism.

Acknowledgements

Supported by National Key Basic Research Science Foundation of China (G2000078404) and National Natural Science Foundation of China (19973009). The authors are grateful to Jack Harvey for his critical reading of the manuscript and valuable suggestions. The authors thank the referee for his criticism, which is very valuable in improving the manuscript. JXW appreciates the kind guidance of Drs López Ariste and Paletou in his learning the QM effects, and allowing him to refer their newly developing papers. They thank Haosheng Lin for valuable discussions. The authors thank the Huairou staff for helping with good observations.

References

Ai, G. and Hu, Y.: 1986, *Publ. Beijing Astron. Obs.* **8**, 1.
Athay, R. G., Querfeld, C. W., Smartt, R. N., Landi Degl'Innocenti, E., and Bommier, V.: 1983, *Solar Phys.* **89**, 3.
Bommier, V. and Leroy, J. L. 1998, *ASP Conf. Series* **150**, 434.
Bommier, V., Leroy, J. L., and Sahal-Bréchot, S.: 1986, *Astron. Astrophys.* **156**, 79.
Brown, A., López Ariste, A., and Casini, R., 2003, *Solar Phys.* (in press).
Foukal, P.: 1998, *ASP Conf. Series* **150**, 446.
Gouttebroze, P., Heinzel, P., and Vial, J.-C.: 1993, *Astron. Astrophys. Suppl. Series* **99**, 513.
Hale, G. E.: 1913, *Astrophys. J.* **38**, 27.
Harvey, J. W.: 1969, Ph.D. Thesis, Colorado University, Colorado.
Heasley, J. N. and Milkey, R. W.: 1978, *Astrophys. J.* **221**, 677.
Heinzel, P., Gouttebroze, P., and Vial, J.-C.: 1987, *Astron. Astrophys.*, **183**, 351.
Kim, I. S., Klepikov, V. Y., Koutchmy, S., Stepanov, A. I., and Stellmacher, G.: 1990, *Soviet Astron. Lett.* **16**, 234.

Kippenhahn, R. and Schlüter, A.: 1957, *Astrophys. J.* **43**, 36.
Kuperus, M. and Raadu, M. A.: 1974, *Astron. Astrophys.* **31**, 189.
Leroy, J. L., Ratier, G., and Bommier, V.: 1977, *Astron. Astrophys.* **54**, 811.
Leroy, J. L., Bommier, V., and Sahal-Bréchot, S.: 1983, *Solar Phys.* **83**, 135.
Leroy, J. L., Bommier, V., and Sahal-Bréchot, S.: 1984, *Astron. Astrophys*. **131**, 33.
Landi Degl'Innocenti, E.: 1982, *Solar Phys.* **79**, 291.
Lin, H., Penn, M. J., and Kuhn, J. R.: 1998, *Astrophys. J.* **493**, 978.
Liu, Y., Wang, J., and Yan, Y.: 1995, *Publ. Beijing Astron. Obs*. **26**, 37.
Low, B. C.: 1996, *Solar Phys*. **167**, 217.
Martin, S. F. and McAllister, A. H.: 1997, in N. Crooker *et al.* (eds.), *Coronal Mass Ejections*, American Geophys. Union, p. 127.
Martin, S. F.: 1998, *ASP Conf. Series* **150**, 419.
Paletou, F., López Ariste, A., Bommier, V., and Semel, M.: 2001, *Astron. Astrophys.*, **375**, L39.
Rust, D. M.: 1967, *Astrophys. J.* **150**, 313.
Rust, D. M. and Kumar, A.: 1994, *Solar Phys.* **155**, 69.
Sánchez Almeida, J.: 1997, *Astron. Astrophys.* **324**, 763.
Tandberg-Hanssen, E.: 1974, *Solar Prominences*, D. Reidel Publ. Co., Dordrecht, Holland.
Tang, F.: 1987, *Solar Phys.* **107**, 233.
Trujillo Bueno, J., Landi Degl'Innocenti, E., Collados, M., Merenda, L., and Manso Sainz, R., 2002, *Nature* **415**, 403.
van Ballegooijen, A.A. 1999, in M. R. Brown *et al.* (eds.), *Magnetic Helicity in Space and Laboratory Plasma, Geophys. Monograph* **111**, 213.
Wang, H., Varsik, J., Zirin, H., Canfield, R. C., Leka, K. D., and Wang, J.: 1992, *Solar Phys.* **142**, 11.
Wang, J. and Shi, Z.: 1983, *Acta Astrophys. Sinica* **3**, 169.
Wang, T., Ai, G., and Deng, Y.: 1996, *Publ. Beijing Astron. Obs.* **28**, 31.
Zhang, H. and Ai, G.: 1987, *Chinese Astron. Astrophys.* **11**, 42.
Zhang, H. and Zhang, M.: 2000, *Solar Phys.* **196**, 269.
Zirin, H. and Severny, A.B.: 1961, *Observatory* **81**, 155.
Zirker, J. B., Martin, S. F., Harvey, K., and Gaizauskas, V.: 1997, *Solar Phys*. **175**, 27.